Journal of Biomechanics 49 (2016) 3289–3297

Contents lists available at ScienceDirect

Journal of Biomechanics

journal homepage: www.elsevier.com/locate/jbiomech
www.JBiomech.com

Valve interstitial cell shape modulates cell contractility independent of cell phenotype

Ishita Tandon [1], Atefeh Razavi [1], Prashanth Ravishankar, Addison Walker, Nasya M. Sturdivant, Ngoc Thien Lam, Jeffrey C. Wolchok, Kartik Balachandran *

Department of Biomedical Engineering, University of Arkansas, Fayetteville, AR 72701, USA

ARTICLE INFO

Article history:
Accepted 11 August 2016

Keywords:
Cell shape
Cell architecture
Contractile stress
Cell phenotype
Valve interstitial cells

ABSTRACT

Valve interstitial cells are dispersed throughout the heart valve and play an important role in maintaining its integrity, function, and phenotype. While prior studies have detailed the role of external mechanical and biological factors in the function of the interstitial cell, the role of cell shape in regulating contractile function, in the context of normal and diseased phenotypes, is not well understood. Thus, the aim of this study was to elucidate the link between cell shape, phenotype, and acute functional contractile output. Valve interstitial cell monolayers with defined cellular shapes were engineered via constraining cells to micropatterned protein lines (10, 20, 40, 60 or 80 μm wide). Samples were cultured in either normal or osteogenic medium. Cellular shape and architecture were quantified via fluorescent imaging techniques. Cellular contractility was quantified using a valve thin film assay and phenotype analyzed via western blotting, zymography, and qRT-PCR. In all pattern widths, cells were highly aligned, with maximum cell and nuclear elongation occurring for the 10 μm pattern width. Cellular contractility was highest for the most elongated cells, but was also increased in cells on the widest pattern (80 μm) that also had increased CX43 expression, suggesting a role for both elongated shape and increased cell-cell contact in regulating contractility. Cells cultured in osteogenic medium had greater expression of smooth muscle markers and correspondingly increased contractile stress responses. Cell phenotype did not significantly correlate with altered cell shape, suggesting that cellular shape plays a significant role in the regulation of valve contractile function independent of phenotype.

© 2016 The Authors. Published by Elsevier Ltd. This is an open access article under the CC BY-NC-ND license (http://creativecommons.org/licenses/by-nc-nd/4.0/).

1. Introduction

Cardiac valves maintain their integrity and function by a complex interplay between the tissue, cells, and surrounding hemodynamic and mechanical environment (Chester and Taylor, 2007). Valve interstitial cells (VICs) are dispersed within the valve leaflets and are crucial in regulating valve matrix composition, function, and disease progression (Taylor et al., 2003). VICs exist as a heterogeneous spectra of phenotypes (Chester and Taylor, 2007; Liu et al., 2007; Taylor et al., 2003). During valve disease, pathogenic stimuli results in activated and osteoblastic phenotypes, potentiating remodeling or further disease progression, respectively (Liu et al., 2007). Another class of smooth-muscle like VICs that appear to be involved in mediating an active contractile response within the tissue (El-Hamamsy et al., 2009; Taylor et al., 2003). Most prior studies have focused on the role of the VIC phenotype in modulating valve function and disease progression. These studies have reported the role of chemical mediators like bone morphogenic proteins, nitric oxide, and the notch pathway in regulating transition to an osteoblastic VIC (Chen et al., 2015; Farrar et al., 2015; Li et al., 2013; Walker et al., 2004; Xu and Gotlieb, 2013). Others have reported the role of mechanical stimulation in potentiating changes in the VIC phenotype (Balachandran et al., 2011, 2009, 2010; Chen et al., 2015; Gould et al., 2013; Hutcheson et al., 2012; Ku et al., 2006; Stephens et al., 2011; Sucosky et al., 2009). An added recent paradigm are the implications of VIC phenotype on its contractile function (Balachandran et al., 2012; El-Hamamsy et al., 2009; Merryman et al., 2006). Relatively few studies discuss the role of VIC shape in regulating its contractile function or biological phenotype.

Cellular shape, enforced by constraining the boundary conditions of cell spreading, potentiates altered cellular function in other cell types. For instance, capillary endothelial cells cultured on single large circles (20 μm) had a significantly greater apoptosis than when cultured on multiple smaller circles (Chen et al., 1997). Rate of proliferation also depended on geometry of the cell

* Correspondence to: Kartik Balachandran, Ph.D., Department of Biomedical Engineering, University of Arkansas, 122 John A. White Jr. Engineering Hall, Fayetteville, AR 72701, USA. Fax: +1 479 575 4346.
E-mail address: kbalacha@uark.edu (K. Balachandran).
[1] Both authors contributed equally.

http://dx.doi.org/10.1016/j.jbiomech.2016.08.013
0021-9290/© 2016 The Authors. Published by Elsevier Ltd. This is an open access article under the CC BY-NC-ND license (http://creativecommons.org/licenses/by-nc-nd/4.0/).

monolayer (Nelson et al., 2005). It was also reported that nuclear shape was regulated by the tension in actomyosin fibers that expanded as cells became more elongated, suggesting an overall balance of intracellular forces (Versaevel et al., 2012). Several recent papers have extended these structural alterations in cells to pro-inflammatory phenotype (McWhorter et al., 2013), cell differentiation (McBeath et al., 2004), and cell motility (Parker et al., 2002). In the context of VICs, it has been acknowledged that VICs alter their shape in response to externally applied mechanical load (Sacks et al., 2009), and that applied load can affect phenotype. In light of these earlier studies, it is therefore important to understand how VICs alter their function and phenotype in response to changes in cell shape and architecture.

We hypothesized that cellular shape directly affects acute contractile function in VICs. To test this hypothesis, we utilized a protein microcontact printing technique (Balachandran et al., 2011) to engineer VIC monolayers constrained with control over cellular shape. VIC contractility was quantified using a valve thin film cantilever assay, and phenotype analyzed via western blots, gelatin zymography, and qRT-PCR. We report that contractility, normalized per cell, was maximum for an elongated cell shape, but also increased in the wider patterns that had increased cell-cell contact as evidenced by increased expression of connexin-43. Cells cultured in osteogenic medium had increased cellular contractility. Cell shape did not have any effect on cell phenotype. Taken as a whole, our results suggest that cell shape plays a significant role in moderating VIC function, and that phenotype measurements alone may not accurately indicate VIC function.

2. Methods

2.1. Valve interstitial cell isolation and culture

Fresh porcine hearts (3–6 months old) were obtained from Cockrum's Custom Meat Processing (Rudy, AR) and transported to our laboratory in cold Dulbecco's Phosphate Buffered Saline (dPBS; Gibco, Carlsbad, CA) supplemented with 1% antibiotic/antimycotic solution. Hearts were immediately dissected aseptically. Left, right, and non-coronary aortic valve leaflets were pooled and washed in Hank's Balanced Salt Solution (HBSS; Gibco). Cells were isolated using collagenase digestion as described in previous protocols (Butcher and Nerem, 2004; Butcher et al., 2004; Gould and Butcher, 2010). Cells from passages 2–6 were used in all subsequent experiments.

2.2. Cell shape model

2.2.1. Photolithography

Photolithographic transparency masks were designed in AutoCAD (Autodesk Inc., San Rafael CA) and fabricated by CAD/Art Services Inc (Bandon, OR). The design of the masks comprised of a regular array of line patterns with five different widths (10, 20, 40, 60, and 80 μm) spaced 40 μm apart. Silicon wafers (Wafer World, West Palm Beach, FL) were then spin coated with Su-8 2005 negative photoresist (MicroChem Corp., Westborough, MA) and exposed to ultraviolet light through the photomask and developed using standard photolithographic protocols (Kane et al., 1999; Qin et al., 2010).

2.2.2. Soft lithography and cell culture

Fibronectin (Corning; 100 μg/mL) was incubated on a polydimethylsiloxane (PDMS; Sylgard 184, Dow Corning) stamped with aforementioned microscale raised patterns for 1 h at room temperature and gently blown dry. The stamp was then placed in contact with Ultraviolet-Ozone (Novascan, Ames, IA) treated PDMS-coated 25 mm no. 1 coverslips for 10 minutes. Coverslips were then blocked for 1 min with 1% Pluronics F-127 (Sigma-Aldrich, St. Louis, MO) to prevent cell attachment onto the areas without fibronectin patterns (Fig. 1A). Fibronectin was chosen for its ease of creating high-fidelity and uniform microscale cell boundaries (Balachandran et al., 2011). Additionally, others have demonstrated that fibronectin did not significantly alter VIC phenotype compared to collagen substrates (Latif et al., 2015). Fibronectin pattern uniformity was also characterized using image analysis techniques familiar to our group (Supplementary Fig. S3) (Balachandran et al., 2011). The coverslips were washed three times with dPBS and VICs were seeded at 100,000 cells per cm^2 coverslip area in normal medium as before or in pro-osteogenic medium (normal culture medium supplemented with 10 mM β-glycerophosphate, 100 nM dexamethasone, and 50 μg/ml ascorbic acid) (Balachandran et al., 2010) and cultured at 37 °C, 5% CO_2. Cells were constrained to the fibronectin patterned portion of the substrate and spontaneously formed confluent monolayers of differing pattern widths within those boundaries (Fig. 1B).

2.3. Characterization of cellular shape and architecture

After 48 h of culture, cells were fixed with 4% PFA/1% Triton X-100 and fluorescently labeled with 1:200 Alexa Fluor 488 phalloidin (Life Technologies, Carlsbad, CA), and 5 μg/mL 4′,6-diamidino-2-phenylindole (DAPI, Life Technologies). Samples were mounted onto a glass slide and imaged using a custom-built resonant-scanning multiphoton microscopy platform with a 40X, 0.8 NA water immersion objective (Nikon, Japan) and a MaiTai ultrafast Ti:Sapphire tunable laser source (Spectra-Physics, Santa Clara, CA). The laser excitation source was tuned to 750 nm (DAPI-stained samples) or 960 nm (Alexa-Fluor 488-stained samples) and images

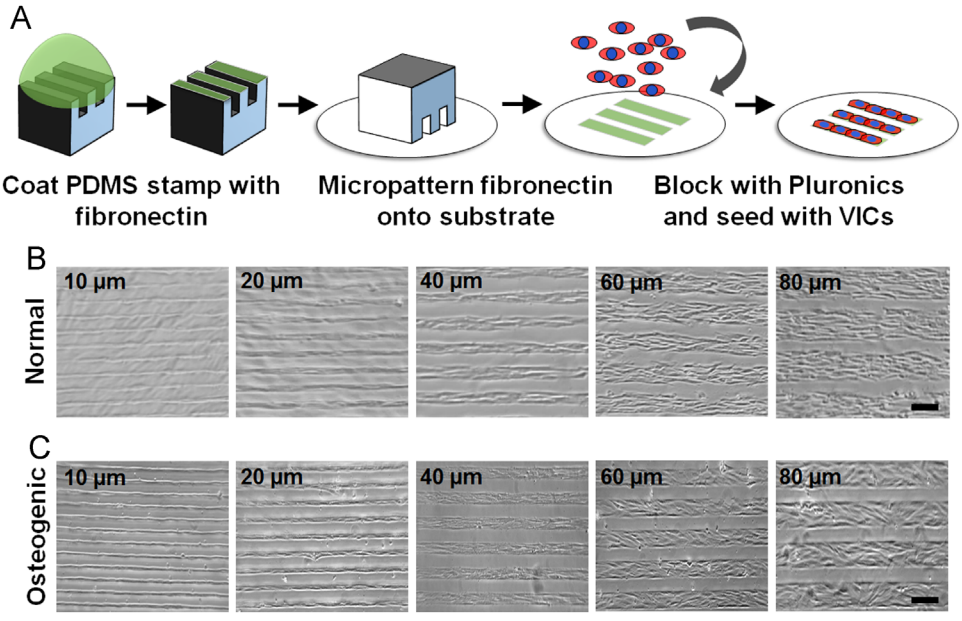

Fig. 1. *In vitro* model for controlling VIC shape. (A) Schematic representation of microcontact printing protocol. Phase contrast microscope images showing formation of VIC micro-tissues in (B) normal and (C) osteogenic media after 48 h of cell culture. (Scale bar = 80 μm).

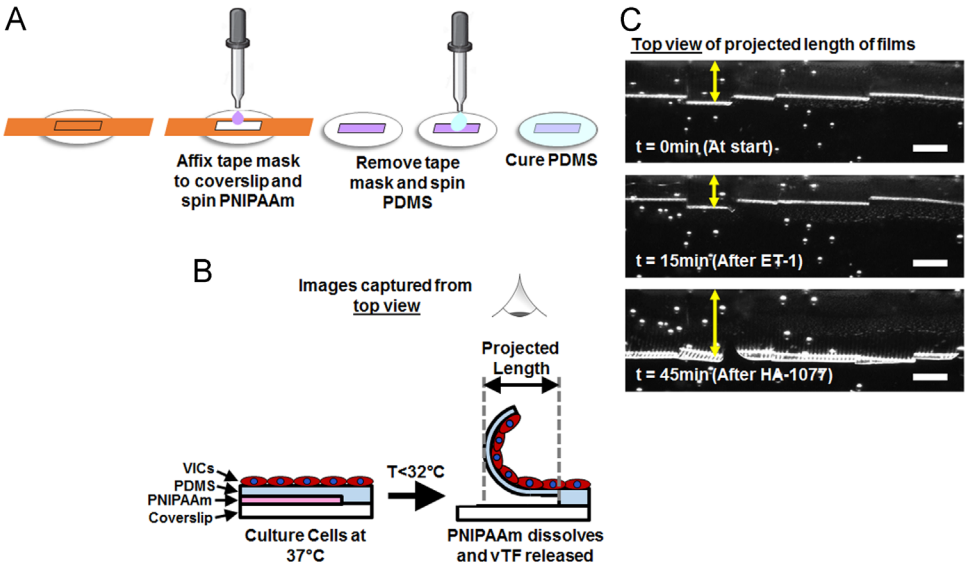

Fig. 2. Valve thin film cantilever experiments. (A) Schematic representation of two-layered substrate preparation for valve thin film cantilever experiments. (B) Schematic representation of dissolution of PNIPAAm layer upon reduction of temperature to < 32 °C and resulting release of VIC and PDMS layers. (C) Representative snapshot of thin film experiments with top-view of films and projected length (yellow arrows) shown at the start of the experiment, after ET-1 stimulation and at the end of the experiment following HA-1077 stimulation. (Scale bars = 1 mm). (For interpretation of the references to color in this figure legend, the reader is referred to the web version of this article.)

were acquired via a 466/40 nm (DAPI) or 525/45 nm (Alexa 488) bandpass filters. Cells from separate experiments were live-stained with 30 μM di-8 ANEPPS (Life Technologies) and imaged using the multiphoton microscope with a 960 nm excitation and via a 607/70 nm emission filter, while being incubated in a coverslip warming chamber (Warner Instruments, Hamden, CT).

Phalloidin stained cells were analyzed using a custom MATLAB script based on a fingerprint detection algorithm to quantify actin filament orientation as a function of different pattern widths (Supplementary Fig. S1) (Balachandran et al., 2011). Termed actin orientation parameter (OP), perfect alignment was indicated by an OP value of 1, while completely isotropic samples had an OP value of 0. Nuclear and cell length-to-width aspect ratios were quantified manually using ImageJ (NIH) analysis of the DAPI images and di-8 stained images, respectively (Bray et al., 2010; Ye et al., 2014). All the above measurements were measured for at least 6 different experimental runs (comprising all pattern widths) from at least 8 fields of view per experimental condition.

2.4. Valve thin film stress measurement assay

Coverslips for valve thin film (vTF) experiments were prepared as previously published by us and others (Alford et al., 2010; Balachandran et al., 2011). Briefly, poly(N-isopropylacrylamide) (PNIPAAm, Sigma-Aldrich) was spin coated onto a 25mm glass coverslip, that had a tape mask (Patco, Flushing, NY) with a rectangular window cut out such that the PNIPAAm would only be coated within this window. The tape mask was removed and PDMS was then spin coated onto the entire coverslip (Fig. 2A). The substrate was cured at 70 °C for 4 h before being micro-contact printed with the pattern widths and cultured as before.

VIC contractile stress and basal tone were calculated using methods published previously (Alford et al., 2010; Balachandran et al., 2011). Briefly, VICs were cultured for 48 h at 37 °C. Before the start of the experiment, culture medium was exchanged with Tyrode's salt solution (Sigma-Aldrich), the VIC and PDMS layers were cut into strips under a stereomicroscope (Leica M205, Leica Microsystems, Wetzlar, Germany), and the sample was allowed to cool to below 32 °C to dissolve the PNIPAAm layer. The PDMS-VIC layer released from the glass as a freely floating cantilever, termed valve thin film (vTF) cantilevers (Fig. 2B). The vTFs would curl due to the inherent tone in the VICs. The vTFs were stimulated with 50 nM endothelin-1 (ET-1; Sigma-Aldrich), followed by an excess dose of 100 μM HA-1077 (Sigma-Aldrich). These doses were determined based on previous studies (Alford et al., 2011; Balachandran et al., 2011; El-Hamamsy et al., 2009). Samples were imaged using the stereomicroscope to record changes in the projected length of the film (x) and calculate the radius of curvature (r) of the cantilever films (Fig. 2C), based on the following:

$$x = \begin{cases} r \sin\left(\frac{L}{r}\right) \in \frac{2L}{\pi} < x < L \\ r \in \frac{L}{2\pi} < x < \frac{2L}{\pi} \end{cases} \quad (1)$$

The stress (σ) required to bend the film was then calculated using the modified Stoney's equation (Feinberg et al., 2007):

$$\sigma = \frac{Et^3}{6r(1-\nu)h^2(1+t/h)} \quad (2)$$

Based on prior publications (Alford et al., 2011; Balachandran et al., 2011), the Young's Modulus of PDMS (E) was assumed to be 1.5 MPa; the Poisson's ratio (ν) of PDMS was assumed to be 0.49; the thickness of the PDMS layer (t) (Supplementary Fig. S2A) was measured using stylus profilometry and the cell layer thickness (h) (Supplementary Fig. S2B) was measured using confocal z-stacks (Balachandran et al., 2011). As the VICs patterned in the wider patterns covered a larger area of the substrate, stress data was normalized by mean cell coverage for each specific pattern as observed under the cell culture microscope (Fig. 1B - C), to yield a normalized stress per cell value. We reported the measurement of VIC contractile stress (response to ET-1), and the basal tone (response to HA-1077). The contractile stress is a measure of the stress generation capacity of the VIC monolayer and is thus a direct measure of cell function (El-Hamamsy et al., 2009). The basal tone is a measure of the baseline stress state of the VICs that was eliminated by HA-1077 relaxation. Sample size was > 20 vTF cantilevers from a minimum of four separate experimental runs for each condition.

2.5. Western blotting and immunostaining

After 48 h of culture, cells were washed three times with sterile dPBS, lysed using RIPA lysis buffer (Santa Cruz, Dallas, TX), and 10 μg of total protein was analyzed via western blotting under reducing conditions, as previously reported (Balachandran et al., 2011). The following primary antibodies were used: Smooth-muscle myosin heavy chain (1:10, Millipore, Billerica, MA), α-smooth muscle actin (1:100, Abcam, Cambridge, MA), vimentin (1:200, Abcam), connexin-43 (CX43; 1:1000, Abcam), and β-actin (1:1000, Abcam). Infrared-conjugated secondary antibodies (1:15000, Li-Cor) were used and samples were imaged using a Li-Cor Odyssey scanner (Li-Cor). Densitometric analysis was performed using the Li-Cor Odyssey software. Band intensity for proteins of interest were normalized with the intensity obtained for β-actin. Sample size was at least n = 5 for each protein.

2.6. Gelatin zymography

Cell lysates were prepared as above and 5 μg of total protein was subjected to gel electrophoresis in a 10% SDS-PAGE gel co-polymerized with 4.67 mg/mL gelatin (Sigma-Aldrich). After renaturation of proteins within the gel, gelatinolytic activities were detected as transparent bands against the background of Coomassie Brilliant Blue stained gels and quantified using ImageJ. Sample size was at least n = 3.

Table 1
List of primers and sequences used in this study (Ku et al., 2006; Lerman et al., 2016).

Target gene	Sense primer sequence	Antisense primer sequence
COL1A1	5-TACCATGACCGAGACGTGTG-3	5-ATAAGACAGCTGGGGAGCAA-3
COL3A1	5-GACATCGAGGATTCCCTGGT-3	5-CCAATCCCAGCAATGGCAG-3
RHOA	5-ACCAGTTCCCA-GAGGTGTATGT −3	5-TTGGGACA-GAAATGCTTGACTTC −3
18S	5-TAGAGGGACAAGTGGCGT-3	5-AATGGGGTTCAACGGGTT-3

2.7. Quantitative real-time polymerase chain reaction

After 48 h of culture, total mRNA was purified using the QIAGEN RNeasy® Plus assay kit (Qiagen, Hilden, Germany), and reverse transcribed to cDNA with iScript RT Supermix (Bio-Rad). Expression of the COL1A1, COL3A1, RHOA, and 18S genes (Table 1) was quantified and analyzed by performing qRT-PCR using the SsoAdvanced™ Universal SYBR Green® supermix (Bio-Rad) with the CFX96™ Real-Time System (BIO-RAD). Expression of the target genes in each sample was reported as dC_t value (relative expression) in reference to the house-keeping gene 18S. Sample size was n=4.

2.8. Statistical analysis

All data were first analyzed for normality using the Anderson–Darling method, and subsequently analyzed by two-way ANOVA followed by Holm-Sidak multiple pairwise comparisons. Data was plotted as mean with standard error bars. Data not normally distributed were analyzed using ANOVA by ranks and Dunn's post-hoc testing, with data plotted as box plots. A p-value of less than 0.05 was used to indicate statistical significance.

3. Results

3.1. In vitro model for altered VIC shape and its implications on cell architecture

Our model demonstrated fine control over cell architecture via constraining the width that VICs were allowed to spread (Fig. 3). We observed that constricting the lateral width of the fibronectin pattern boundaries, as in the narrow 10 and 20 μm line patterns, resulted in cells forming exaggerated, elongated shapes with highly aligned actin architecture (Fig. 3A and B). Wider pattern boundaries (60 and 80 μm) resulted in cells that maintained the spindle-like shape of a VIC, but with lower length-to-width aspect ratios and actin architecture that was more variable in alignment (Fig. 3A and B). Quantification of actin alignment using the orientation parameter (OP) (Fig. 3C) indicated that 10 and 20 μm wide VICs had significantly greater actin cytoskeletal alignment compared to 40, 60 and 80 μm wide ones ($^*p < 0.05$). VICs cultured in osteogenic media had lower actin OP values compared to corresponding samples cultured in normal media, suggesting greater disorder in the cytoskeletal architecture.

Cell aspect ratio measurements (Fig. 3D) demonstrated similar results as the actin OP, with 10 and 20 μm wide VICs having significantly higher length-to-width aspect ratios compared to wider pattern widths in both normal and osteogenic conditions ($^*p < 0.05$). Similarly, nuclear aspect ratios (Fig. 3E) in 10 and 20 μm wide VIC monolayers were statistically greater than the wider pattern widths ($^*p < 0.05$). In line with the actin OP data, nuclear aspect ratios of VICs cultured in normal media were higher than that of VICs cultured in osteogenic media ($^*p < 0.05$). Additionally, the nuclear aspect ratio values were within a tighter range compared to the cellular aspect ratios, with the median values for all pattern widths falling between 1.6 and 3.4 for nuclear aspect ratio and between 6.8 and 9.5 for cell aspect ratio. Nuclear aspect ratios were also highly correlated with cellular aspect ratios (Fig. 3F).

3.2. VIC contractile function was modulated by cell shape

All samples in both normal and osteogenic media demonstrated an acute contractile response to ET-1 and a vasodilatory response to HA-1077 (Fig. 4A and B; Supplementary Videos S1-S10). Analysis of maximum induced contraction (Fig. 4C) revealed a U-shaped response with respect to VIC pattern width for both normal and osteogenic VICs. We observed significantly decreasing contractile stress with increasing pattern width until low contraction values were reached at the 40 and 60 μm widths ($^*p < 0.05$). Subsequent increase in VIC pattern width to 80 μm resulted in significantly increased maximum contractile stress ($^*p < 0.05$). We noted significantly increased contractile stress response for every pattern width in the osteogenic VICs compared to the similarly patterned VICs cultured in normal media ($^*p < 0.05$). The rate of contraction (Fig. 4D) followed a similar trend as the contraction data (Fig. 4C). Osteogenic VICs demonstrated significantly faster rates of contraction ($^*p < 0.05$). Taken together, the peak stress and contraction rate data suggest that osteogenic VIC contraction is both more robust and faster than normal VICs. Additionally, similar U-shaped response curves were observed for all pattern widths.

Supplementary material related to this article can be found online at http://dx.doi.org/10.1016/j.jbiomech.2016.08.013.

VIC response to HA-1077 (Fig. 4E) revealed no significant differences in cellular basal tone as a function of VIC pattern width for normal VICs. Within osteogenic VICs, we observed significantly increased basal tone for the 10 μm and 80 μm pattern widths, compared to both the corresponding normal VICs with the same pattern widths, as well as the 20, 40 and 60 μm osteogenic VICs ($^*p < 0.05$).

3.3. VIC phenotype was not affected by altered cell shape

Western blotting (Fig. 5A) together with semi-quantitative densitometric analysis revealed that cell shape did not have a significant effect ($p > 0.05$) on VIC phenotype. Changes in pattern width did not significantly alter the expression of vimentin (Fig. 5A), SM-MHC (Fig. 5B) or α-SMA (Fig. 5C), suggesting that there was consistent expression of the myofibroblast and smooth muscle-like phenotype across all VIC pattern widths. Culture conditions (normal vs. osteogenic), however, had a significant effect ($^*p < 0.05$) on VIC phenotype. Osteogenic media resulted in a significant increase in both SM-MHC (Fig. 5B), and α-SMA (Fig. 5C) expression compared to corresponding normal media conditions ($^*p < 0.05$). CX43 expression (Fig. 5D) was significantly increased ($^*p < 0.05$) as a function of increasing pattern width as well as in osteogenic VICs, suggesting an overall increase in normalized cell-cell contact with increasing pattern width, and in osteogenic conditions.

MMP-2 gelatinolytic activity (Fig. 6A and B) showed a similar trend, where culture conditions had a significant effect ($^*p < 0.05$) on MMP-2 activity, while increasing pattern width did not. Additionally, the MMP-2 was in the active form only for the osteogenic conditions and not the normal culture conditions (Fig. 6A), suggesting greater remodeling activity in the osteogenic VICs. COL1A1, COL3A1 and RhoA gene expression (Supplementary Fig. S4) were not significantly altered as a function of pattern width or osteogenic culture medium.

4. Discussion

Over the last decade, extensive research has implicated biochemical mediators, the mechanical environment, and the

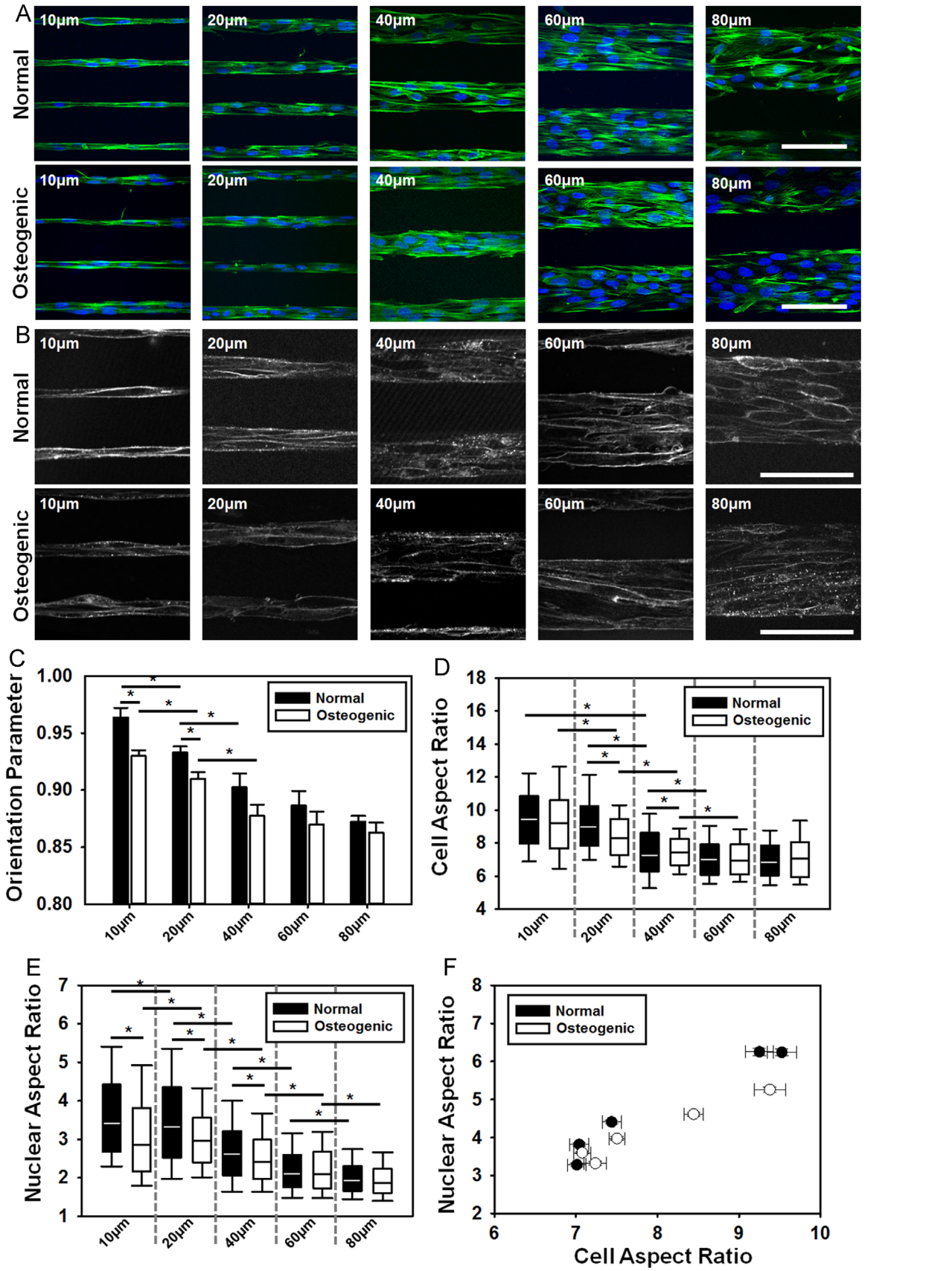

Fig. 3. Constraining VIC boundaries altered cell shape and architecture. (A) Phalloidin (green) and DAPI (blue) stained images of VIC micro-tissues constrained to different pattern widths, cultured in normal and osteogenic media. (Scale bar = 80μm) (B) Di-8 (white) stained VIC micro-tissues. (Scale bar = 80μm) (C) Actin orientation parameter, (D) cell aspect ratio, and (E) nuclear aspect ratio data for all VIC micro-tissue pattern widths. ($^*p < 0.05$) (F) Correlation between nuclear and cell aspect ratio (Black circles – normal; White circles – osteogenic; Pearson correlation: r = 0.935, p = 7.13e − 5). (For interpretation of the references to color in this figure legend, the reader is referred to the web version of this article.)

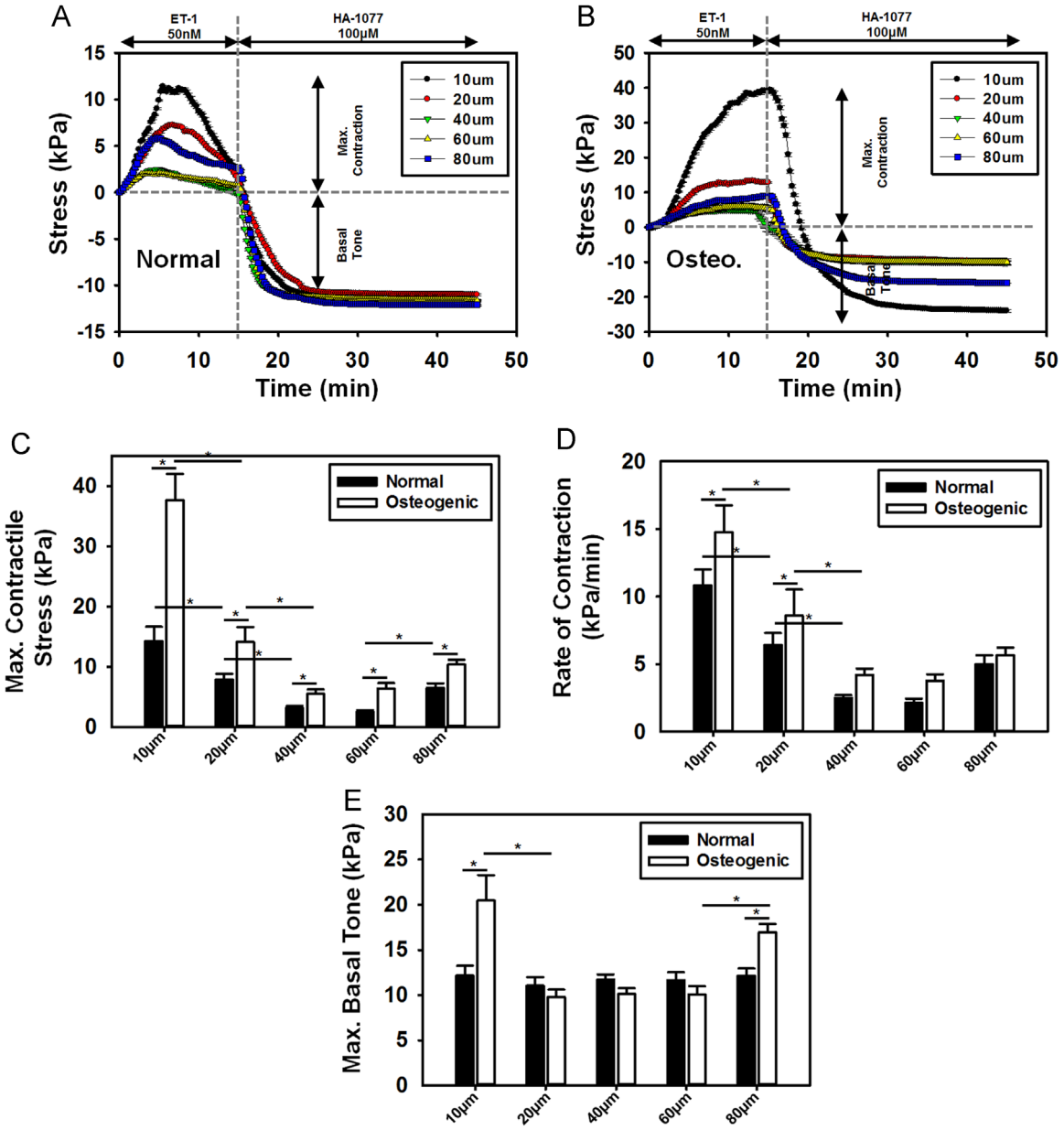

Fig. 4. VIC shape influenced cellular contractile function. Stress-time plots for 10, 20, 40, 60 and 80 μm VIC micro-tissues in (A) normal and (B) osteogenic culture medium, normalized to a per cell basis. (C) Maximum VIC micro-tissue contraction induced by 50 nM ET-1 stimulation. (D) Rate of contraction due to ET-1 stimulation. (E) Maximum basal tone within VIC micro-tissues induced by 100 μM HA-1077 stimulation. ($^*p < 0.05$).

substrate as factors that regulate the VIC phenotype and function (Balachandran et al., 2011, 2009, 2010; Chen et al., 2015; Gould et al., 2013; Hutcheson et al., 2012; Ku et al., 2006; Liu et al., 2013; Quinlan and Billiar, 2012; Stephens et al., 2011; Sucosky et al., 2009; Wang et al., 2013; Yip and Simmons, 2011). In the current study, we used micropatterned VICs with enforced shapes via constraining boundary conditions to study the relationship between cell shape and contractile output. Our results suggest that alteration of VIC shape alone can modulate contractile output, even in the absence of contractile markers. Indeed, while the extracellular matrix substrate components such as collagen and elastin have a major role in modulating the mechanics of the whole valve (Rodriguez et al., 2014), our results suggest an important role for smaller scale geometric variations in VICs as well. Future studies will investigate the interaction between cellular shape and other factors such as substrate stiffness or externally applied mechanically load in modulating VIC function.

Traditionally, the study of VICs has lacked a robust *in vitro* functional assay to complement molecular biology-based techniques that quantify smooth muscle, myofibroblast, and fibroblast protein expression to indicate VIC phenotype. The vTF cantilever assay presented here allows direct measurements of cellular contractile output. This assay can potentially be extended to test the role of other contractile mediators on valve function as a complement to earlier *ex vivo* studies (Balachandran et al., 2011; El-Hamamsy et al., 2009). Utilizing this vTF assay, our most significant finding was that VICs cultured in both the narrower (10 μm) and wider patterns (80 μm) exhibited strong induced contractile responses to ET-1. These responses were not associated with corresponding changes in VICs phenotype or remodeling markers. It is possible that the increased contractile response in the wider patterns (80μm) can be attributed to increased cell-cell contact as evidenced by the increased CX43 expression in these samples. Within the VICs treated with osteogenic medium, contractility was modulated by cell shape in a similar

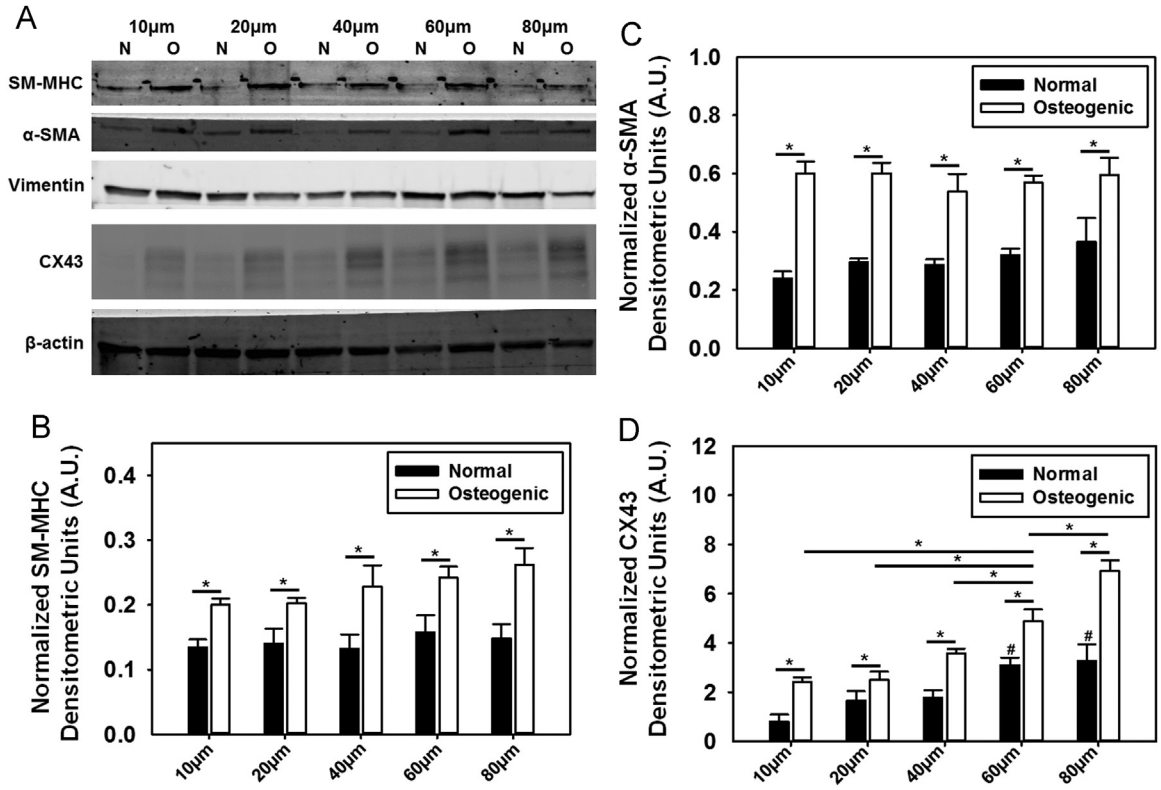

Fig. 5. Western blotting analysis of VIC phenotype. (A) Representative western blots of smooth muscle myosin heavy chain (SM-MHC), α-smooth muscle actin (α-SMA), vimentin, connexin-43 (CX43) and β-actin loading control. Semi-quantitative analysis of western blot band densitometry of (B) SM-MHC, (C) α-SMA, and (D) CX43. (*$p < 0.05$).

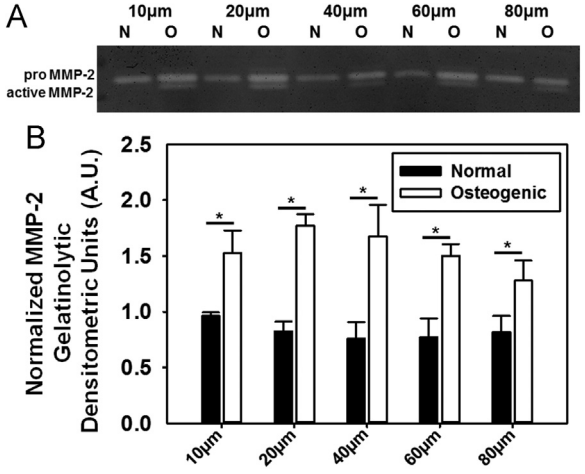

Fig. 6. Gelatin zymography analysis. (A) Representative gelatin zymogram image. (B) Semi-quantitative analysis of gelatinolytic activity. (*$p < 0.05$).

manner to the normal VICs, with values significantly higher in osteogenic VICs. This last result is all the more intriguing, as osteogenic VICs had lower metrics for actin alignment and cellular elongation compared to the corresponding normal VICs, and is likely related to the increased expression of activated phenotype markers, as well as cell-cell contact markers, in the osteogenic VICs. The contractile response results, taken together with the cellular shape results, suggested that induced contractile stress was regulated by a combination of cell aspect ratio, which was maximized in the narrower patterns, and cell-cell contact within a pattern, maximized in the wider patterns. Taken as a whole, these results strongly suggests that phenotype marker measurements might not be sufficient to characterize the contractile function of the VIC, and that additional direct functional measurements have to be employed.

Recent publications have indicated cellular functional and pathological behavior as an emergent property that can be dictated by structural shape and architectural organization in other cell types, including vascular smooth muscle cells and cardiomyocytes (Alford et al., 2011; Lee et al., 2015; Parker and Ingber, 2007; Parker et al., 2008; Tee et al., 2011; Win et al., 2014). Changes in striated muscle morphology within the heart have been associated with contractile dysfunction (Gerdes, 2002). Internally generated contractile stresses also deformed the myocyte nucleus (Bray et al., 2010). Additionally, vascular smooth muscle cells demonstrate altered contractile behavior depending on cellular elongation (Alford et al., 2011; Win et al., 2014). Unfortunately, studies relating VIC morphology to valvular function and disease are limited. Elongated VICs were reported to be more motile (Liu and Gotlieb, 2007). Lengthening of VIC nuclear and cellular shape was also correlated with increased mechanical strain within the valve tissue (Sacks et al., 2009). While it would be speculative to compare the elongated shapes in our model to the elongated shapes observed in stretched valve leaflets, it was reported that VICs under elevated strain also generated increased contractile stress (Balachandran et al., 2012), as seen in this study.

Our observed correlation between nuclear and cell shape was expected, as the cell membrane and the cytoskeleton are interconnected with the nuclear lamina (Dahl et al., 2008). Indeed, it was recently reported that cell elongation of singly microcontact printed cells potentiated a more elongated but laterally-compact nucleus (Versaevel et al., 2012). The change in nuclear shape was thought to be due to lateral compression by stress fibers. Further, it has been proposed that nuclear deformation by cytoskeletal forces plays a key role in mechanotransduction (Dahl et al., 2008; Wang

et al., 2009). It is thus possible that nuclear mechanics also play an important role in regulating VIC function.

Finally, we show in this study that controlling VIC structure can be used to finely tune the functional behavior of the cell. In addition to providing mechanical insights into the structure-function relationship of VICs, our finding is of particular importance to the field of valvular tissue engineering, where there is a need to direct cellular function to yield a viable and functional valve replacement (Mack, 2014; Vesely, 2005). Our study thus suggests that providing organizational cues in addition to chemical and mechanical stimuli might be beneficial in the development of a tissue-engineered replacement valve.

Conflict of interest statement

The authors declare that there are no financial or commercial conflicts of interest to report.

Acknowledgments

This material is based upon work supported by the National Science Foundation under Grant No. CMMI-1452943 (K.B.) and the Arkansas Biosciences Institute Grant 000943 (K.B.). We thank Dr. Timothy Muldoon for his assistance with the multiphoton microscope. We also acknowledge the University of Arkansas High Density Electronics Center (HiDEC) and their staff for technical assistance with the microfabrication work.

Appendix A. Supporting information

Supplementary data associated with this article can be found in the online version at http://dx.doi.org/10.1016/j.jbiomech.2016.08.013.

References

Alford, P.W., Feinberg, A.W., Sheehy, S.P., Parker, K.K., 2010. Biohybrid thin films for measuring contractility in engineered cardiovascular muscle. Biomaterials 31, 3613–3621.
Alford, P.W., Nesmith, A.P., Seywerd, J.N., Grosberg, A., Parker, K.K., 2011. Vascular smooth muscle contractility depends on cell shape. Integr. Biol. Quant. Biosci. nano Macro 3, 1063–1070.
Balachandran, K., Sucosky, P., Jo, H., Yoganathan, A.P., 2009. Elevated cyclic stretch alters matrix remodeling in aortic valve cusps: implications for degenerative aortic valve disease. Am. J. Physiol. Heart Circ. Physiol. 296, H756–H764.
Balachandran, K., Sucosky, P., Jo, H., Yoganathan, A.P., 2010. Elevated cyclic stretch induces aortic valve calcification in a bone morphogenic protein-dependent manner. Am. J. Pathol. 177, 49–57.
Balachandran, K., Hussain, S., Yap, C.H., Padala, M., Chester, A.H., Yoganathan, A.P., 2012. Elevated cyclic stretch and serotonin result in altered aortic valve remodeling via a mechanosensitive 5-HT(2A) receptor-dependent pathway. Cardiovasc. Pathol. Off. J. Soc. Cardiovasc. Pathol. 21, 206–213.
Balachandran, K., Alford, P.W., Wylie-Sears, J., Goss, J.A., Grosberg, A., Bischoff, J., Aikawa, E., Levine, R.A., Parker, K.K., 2011. Cyclic strain induces dual-mode endothelial-mesenchymal transformation of the cardiac valve. Proc. Natl. Acad. Sci. USA 108, 19943–19948.
Bray, M.A., Adams, W.J., Geisse, N.A., Feinberg, A.W., Sheehy, S.P., Parker, K.K., 2010. Nuclear morphology and deformation in engineered cardiac myocytes and tissues. Biomaterials 31, 5143–5150.
Butcher, J.T., Nerem, R.M., 2004. Porcine aortic valve interstitial cells in three-dimensional culture: comparison of phenotype with aortic smooth muscle cells. J Heart Valve Dis. 13 (478–485), 485 476.
Butcher, J.T., Penrod, A.M., Garcia, A.J., Nerem, R.M., 2004. Unique morphology and focal adhesion development of valvular endothelial cells in static and fluid flow environments. Arterioscler. Thromb. Vasc. Biol. 24, 1429–1434.
Chen, C.S., Mrksich, M., Huang, S., Whitesides, G.M., Ingber, D.E., 1997. Geometric control of cell life and death. Science 276, 1425–1428.
Chen, J., Ryzhova, L.M., Sewell-Loftin, M.K., Brown, C.B., Huppert, S.S., Baldwin, H.S., Merryman, W.D., 2015. Notch1 mutation leads to valvular calcification through enhanced myofibroblast mechanotransduction. Arterioscler. Thromb. Vasc. Biol. 35, 1597–1605.
Chester, A.H., Taylor, P.M., 2007. Molecular and functional characteristics of heart-valve interstitial cells. Philos. Trans. R. Soc. Lond. 362, 1437–1443.
Dahl, K.N., Ribeiro, A.J., Lammerding, J., 2008. Nuclear shape, mechanics, and mechanotransduction. Circ. Res. 102, 1307–1318.
El-Hamamsy, I., Balachandran, K., Yacoub, M.H., Stevens, L.M., Sarathchandra, P., Taylor, P.M., Yoganathan, A.P., Chester, A.H., 2009. Endothelium-dependent regulation of the mechanical properties of aortic valve cusps. J Am. Coll. Cardiol. 53, 1448–1455.
Farrar, E.J., Huntley, G.D., Butcher, J., 2015. Endothelial-derived oxidative stress drives myofibroblastic activation and calcification of the aortic valve. PLoS One 10, e0123257.
Feinberg, A.W., Feigel, A., Shevkoplyas, S.S., Sheehy, S., Whitesides, G.M., Parker, K.K., 2007. Muscular thin films for building actuators and powering devices. Science 317, 1366–1370.
Gerdes, A.M., 2002. Cardiac myocyte remodeling in hypertrophy and progression to failure. J. Card. Fail. 8, S264–S268.
Gould, R.A., Butcher, J.T., 2010. Isolation of valvular endothelial cells. J. Vis. Exp.
Gould, S.T., Srigunapalan, S., Simmons, C.A., Anseth, K.S., 2013. Hemodynamic and cellular response feedback in calcific aortic valve disease. Circ. Res. 113, 186–197.
Hutcheson, J.D., Venkataraman, R., Baudenbacher, F.J., Merryman, W.D., 2012. Intracellular Ca(2+) accumulation is strain-dependent and correlates with apoptosis in aortic valve fibroblasts. J. Biomech. 45, 888–894.
Kane, R.S., Takayama, S., Ostuni, E., Ingber, D.E., Whitesides, G.M., 1999. Patterning proteins and cells using soft lithography. Biomaterials 20, 2363–2376.
Ku, C.H., Johnson, P.H., Batten, P., Sarathchandra, P., Chambers, R.C., Taylor, P.M., Yacoub, M.H., Chester, A.H., 2006. Collagen synthesis by mesenchymal stem cells and aortic valve interstitial cells in response to mechanical stretch. Cardiovasc. Res. 71, 548–556.
Latif, N., Quillon, A., Sarathchandra, P., McCormack, A., Lozanoski, A., Yacoub, M.H., Chester, A.H., 2015. Modulation of human valve interstitial cell phenotype and function using a fibroblast growth factor 2 formulation. PLoS One 10, e0127844.
Lee, H., Adams, W.J., Alford, P.W., McCain, M.L., Feinberg, A.W., Sheehy, S.P., Goss, J.A., Parker, K.K., 2015. Cytoskeletal prestress regulates nuclear shape and stiffness in cardiac myocytes. Exp. Biol. Med.
Lerman, D.A., Prasad, S., Alotti, N., 2016. Using Na3PO4 to Enhance In vitro Animal Models of Aortic Valve Calcification. Int. J. Cardiovasc. Res., 5.
Li, C., Xu, S., Gotlieb, A.I., 2013. The progression of calcific aortic valve disease through injury, cell dysfunction, and disruptive biologic and physical force feedback loops. Cardiovasc. Pathol. Off. J. Soc. Cardiovasc. Pathol. 22, 1–8.
Liu, A.C., Gotlieb, A.I., 2007. Characterization of cell motility in single heart valve interstitial cells in vitro. Histol. Histopathol. 22, 873–882.
Liu, A.C., Joag, V.R., Gotlieb, A.I., 2007. The emerging role of valve interstitial cell phenotypes in regulating heart valve pathobiology. Am. J. Pathol. 171, 1407–1418.
Liu, H., Sun, Y., Simmons, C.A., 2013. Determination of local and global elastic moduli of valve interstitial cells cultured on soft substrates. J. Biomech. 46, 1967–1971.
Mack, M., 2014. Progress toward tissue-engineered heart valves. J. Am. Coll. Cardiol. 63, 1330–1331.
McBeath, R., Pirone, D.M., Nelson, C.M., Bhadriraju, K., Chen, C.S., 2004. Cell shape, cytoskeletal tension, and RhoA regulate stem cell lineage commitment. Dev. cell 6, 483–495.
McWhorter, F.Y., Wang, T., Nguyen, P., Chung, T., Liu, W.F., 2013. Modulation of macrophage phenotype by cell shape. Proc. Natl. Acad. Sci. USA 110, 17253–17258.
Merryman, W.D., Huang, H.Y., Schoen, F.J., Sacks, M.S., 2006. The effects of cellular contraction on aortic valve leaflet flexural stiffness. J. Biomech. 39, 88–96.
Nelson, C.M., Jean, R.P., Tan, J.L., Liu, W.F., Sniadecki, N.J., Spector, A.A., Chen, C.S., 2005. Emergent patterns of growth controlled by multicellular form and mechanics. Proc. Natl. Acad. Sci. USA 102, 11594–11599.
Parker, K.K., Ingber, D.E., 2007. Extracellular matrix, mechanotransduction and structural hierarchies in heart tissue engineering. Philos. Trans. R. Soc. Lond. 362, 1267–1279.
Parker, K.K., Tan, J., Chen, C.S., Tung, L., 2008. Myofibrillar architecture in engineered cardiac myocytes. Circ. Res 103, 340–342.
Parker, K.K., Brock, A.L., Brangwynne, C., Mannix, R.J., Wang, N., Ostuni, E., Geisse, N.A., Adams, J.C., Whitesides, G.M., Ingber, D.E., 2002. Directional control of lamellipodia extension by constraining cell shape and orienting cell tractional forces. FASEB J. 16, 1195–1204.
Qin, D., Xia, Y., Whitesides, G.M., 2010. Soft lithography for micro- and nanoscale patterning. Nat. Protoc. 5, 491–502.
Quinlan, A.M., Billiar, K.L., 2012. Investigating the role of substrate stiffness in the persistence of valvular interstitial cell activation. J Biomed. Mater. Res A 100, 2474–2482.
Rodriguez, K.J., Piechura, L.M., Porras, A.M., Masters, K.S., 2014. Manipulation of valve composition to elucidate the role of collagen in aortic valve calcification. BMC Cardiovasc. Disord. 14, 29.
Sacks, M.S., David Merryman, W., Schmidt, D.E., 2009. On the biomechanics of heart valve function. J. Biomech. 42, 1804–1824.
Stephens, E.H., Durst, C.A., West, J.L., Grande-Allen, K.J., 2011. Mitral valvular interstitial cell responses to substrate stiffness depend on age and anatomic region. Acta Biomater. 7, 75–82.
Sucosky, P., Balachandran, K., Elhammali, A., Jo, H., Yoganathan, A.P., 2009. Altered shear stress stimulates upregulation of endothelial VCAM-1 and ICAM-1 in a

BMP-4- and TGF-beta1-dependent pathway. Arterioscler. Thromb. Vasc. Biol. 29, 254–260.
Taylor, P.M., Batten, P., Brand, N.J., Thomas, P.S., Yacoub, M.H., 2003. The cardiac valve interstitial cell. Int. J. Biochem. Cell Biol. 35, 113–118.
Tee, S.Y., Fu, J., Chen, C.S., Janmey, P.A., 2011. Cell shape and substrate rigidity both regulate cell stiffness. Biophys. J. 100, L25–L27.
Versaevel, M., Grevesse, T., Gabriele, S., 2012. Spatial coordination between cell and nuclear shape within micropatterned endothelial cells. Nat. Commun. 3, 671.
Vesely, I., 2005. Heart valve tissue engineering. Circ. Res. 97, 743–755.
Walker, G.A., Masters, K.S., Shah, D.N., Anseth, K.S., Leinwand, L.A., 2004. Valvular myofibroblast activation by transforming growth factor-beta: implications for pathological extracellular matrix remodeling in heart valve disease. Circ. Res. 95, 253–260.
Wang, H., Tibbitt, M.W., Langer, S.J., Leinwand, L.A., Anseth, K.S., 2013. Hydrogels preserve native phenotypes of valvular fibroblasts through an elasticity-regulated PI3K/AKT pathway. Proc. Natl. Acad. Sci. USA 110, 19336–19341.
Wang, N., Tytell, J.D., Ingber, D.E., 2009. Mechanotransduction at a distance: mechanically coupling the extracellular matrix with the nucleus. Nat. Rev. Mol. Cell Biol. 10, 75–82.
Win, Z., Vrla, G.D., Steucke, K.E., Sevcik, E.N., Hald, E.S., Alford, P.W., 2014. Smooth muscle architecture within cell-dense vascular tissues influences functional contractility. Integr. Biol. Quant. Biosci. Nano Macro 6, 1201–1210.
Xu, S., Gotlieb, A.I., 2013. Wnt3a/beta-catenin increases proliferation in heart valve interstitial cells. Cardiovasc. Pathol. Off. J. Soc. Cardiovasc. Pathol. 22, 156–166.
Ye, G.J., Aratyn-Schaus, Y., Nesmith, A.P., Pasqualini, F.S., Alford, P.W., Parker, K.K., 2014. The contractile strength of vascular smooth muscle myocytes is shape dependent. Integr. Biol. : Quant. Biosci. Nano Macro 6, 152–163.
Yip, C.Y., Simmons, C.A., 2011. The aortic valve microenvironment and its role in calcific aortic valve disease. Cardiovasc. Pathol. 20, 177–182.